JOURNAL OF GUIDANCE, CONTROL, AND DYNAMICS
Vol. 32, No. 3, May–June 2009

Sequential Traffic Flow Optimization with Tactical Flight Control Heuristics

Shon Grabbe* and Banavar Sridhar†
NASA Ames Research Center, Moffett Field, California 94035-1000
and
Avijit Mukherjee‡
University of California, Santa Cruz, Moffett Field, California 94035-1000

DOI: 10.2514/1.40300

A sequential optimization method is applied to manage air traffic flow under uncertainty in airspace capacity and demand. To support its testing, a decision support system is developed by integrating a deterministic integer programming model for assigning delays to aircraft under en route capacity constraints with a fast-time simulation environment to reactively account for system uncertainties. To reduce computational complexity, the model assigns only departure controls, and a tactical control loop consisting of a shortest-path routing algorithm and an airborne-delay algorithm refines the strategic plan to keep flights from deviating into capacity-constrained airspace. This integrated approach was used to conduct 32 six-hour fast-time simulation experiments to explore variations in the number and severity of departure controls, tactical reroutes, and airborne-delay controls. These experiments highlighted a fundamental difference in the manner in which weather translation is performed at the strategic and tactical levels. Although tactical weather translation explicitly accounts for the direct impact of weather on individual flights, strategic weather translation, which is accomplished by calculating a reduced capacity for a region of airspace such as a sector, typically fails to account for these flow-based impacts. Finally, an initial validation of the rerouting algorithm, which was the dominant control strategy for avoiding en route weather in the experiments, indicates that the algorithm is able to generate reroutes that are, on average, shorter than operationally flown weather-avoidance routes, when regions of airspace that flights are likely to avoid are identified using the convective-weather-avoidance model.

Nomenclature

$A_k(t)$	=	time-varying arrival capacity of airport $k \in K$
$D_k(t)$	=	time-varying departure capacity of airport $k \in K$
d_f	=	scheduled start time of flight f
F	=	set of flights
G	=	maximum amount of delay that can be assigned per flight
J	=	set of sectors
K	=	set of airports
$l_{f,j}$	=	amount of time flight f is required to spend in sector j
N_f	=	number of resources (i.e., sectors and airports) in the path of flight f
$P(f,i)$	=	ith sector used by flight f, $P(f,i) \in J$
$S_j(t)$	=	time-varying sector capacity
T	=	number of discrete time intervals that constitute the planning horizon

I. Introduction

TRAFFIC flow management (TFM) in the United States consists of two loosely coupled phases under current-day operations. In the first phase, the Federal Aviation Administration's (FAA's) Air Traffic Control System Command Center (ATCSCC) develops national-level flow management initiatives over a 2–8 h planning horizon. The second phase, which is performed at the center level over a 30-min-to-2-h time horizon, serves as a tactical control loop to implement the national-level initiatives and to introduce local flow control initiatives, such as miles-in-trail and tactical rerouting. These center-level controls are designed to accommodate localized disturbances in the National Airspace System (NAS) or to refine the national-level plan in response to updated weather and traffic information [1,2]. Aside from a limited number of decision support capabilities, such as the enhanced traffic management system (ETMS) [3] and the flight schedule monitor [4], the daunting task of developing national and tactical flow control programs is largely left to human operators, who rely on a combination of intuition and past experience. This can result in the under- or over- and inconsistent controlling of traffic flows and the inability to accommodate user preferences. With capacity limited by controller workload in many parts of the country and with the forecasted doubling or tripling of air traffic in the United States over the next 20 years [5], there is a need to develop advanced automation that can maximize the throughput and efficiency of the NAS while accommodating user preferences under sources of uncertainty, such as weather.

To address this research gap, a number of recent studies have proposed methods to facilitate the development of TFM controls in the 30-min-to-8-h time horizon [6–10]. In [6], an integrated three-step hierarchical method is proposed for developing deterministic TFM plans, consisting of national-level playbook reroutes, miles-in-trail restrictions, and tactical reroutes to alleviate sector-level congestion. A deterministic center-based system that can be used to manually identify congested sectors and compare the tradeoffs of implementing altitude capping, local rerouting, departure delays, and time-based metering or miles-in-trail restrictions is proposed in [7]. A deterministic open-loop integer-programming-based model that can be used to assign departure delays, airborne delays, and reroutes to individual flights is proposed in [8], but the computational complexity of this model has limited its use to a small number of real-world examples [11]. Finally, [9] proposes a Monte Carlo-based,

Presented as Paper 6823 at the AIAA Guidance, Navigation, and Control Conference, Honolulu, HI, 18–21 August 2008; received 6 August 2008; revision received 23 December 2008; accepted for publication 24 December 2008.

*Research Scientist, Automation Concepts Research Branch, Mail Stop 210-10; shon.r.grabbe@nasa.gov. Senior Member AIAA.
†Senior Scientist, Aviation Systems Division, Mail Stop 210-10. Fellow AIAA.
‡Associate Project Scientist, Mail Stop 210-8.

incremental, probabilistic decision-making approach for developing en route traffic management controls. A key research gap that has yet to be addressed is determining how the promising optimization-based approach proposed in [8] can be exploited for developing TFM controls that account for system uncertainties, while overcoming the documented computational complexities associated with this approach [11].

To begin addressing this research gap, [10] proposed a sequential optimization approach that integrates a strategic departure control model with a fast-time simulation environment to reactively control flights subject to system uncertainties, such as imperfect weather and flight intent information. This departure control model is formulated as a deterministic integer programming model, which assigns predeparture delays to individual flights based on deterministic estimates of the flight schedule, airport capacities, and airspace capacities. Tactical flight controls in the form of weather-avoidance reroutes and airborne delays are subsequently implemented directly within the simulation through a combination of heuristic- and optimization-based techniques to refine the strategic plan to account for system uncertainties. The current study further refines this sequential optimization approach:

1) Dijkstra's algorithm [12] is implemented to generate computationally efficient weather-avoidance reroutes.

2) A refined en route weather translation model [13] is implemented.

3) An initial validation of the model-estimated delay metrics is provided.

Section II describes the strategic and tactical models adopted in this study for assigning departure delays, tactical reroutes, and airborne delays to flights. The software simulation environment that was developed to support the sequential decision-making model is also described in Sec. II. A discussion of the flight schedules, weather scenarios, and airspace capacity constraints used in this study is presented in Sec. III. The frequency and intensity of the departure, rerouting, and airborne-delay controls are presented in Sec. IV. Additionally, Sec. IV provides the results of an initial validation of the model-estimated delay metrics. Finally, concluding remarks are presented in Sec. V.

II. Modeling Method

This section describes the integrated optimization-simulation architecture. After first describing its key attributes, a modification of the binary integer programming model described in [8] is presented. Following this discussion, the weather-avoidance rerouting algorithm and the airborne-delay algorithm are described.

A. System Architecture

The major components of the Java-based integrated optimization-simulation environment are illustrated in Fig. 1. To the left of this image are the system inputs, which consist of user schedules and flight plans, weather data, and airspace adaptation data. For this study, the user schedules and adaptation data are extracted from historical ETMS data archives that will be described in Sec. III. The primary source of weather was from the convective-weather-avoidance model (CWAM) [13], which translates raw meteorological data such as precipitation intensity and echo top height into regions of airspace that pilots are likely to deviate around. The use of this data source is described in more detail in Sec. III.

These system inputs were processed directly by the primary simulation system that was chosen to be NASA's Future ATM Concepts Evaluation Tool (FACET) [14]. Every minute, the primary simulation provides updated state information $x(t)$ (e.g., latitude, longitude, speed, altitude, and heading) for all aircraft in the simulation, and updates to the weather data $w(t)$ are provided every 5 min, which corresponds to the frequency at which updates to the CWAM deviation probability contours are received.

Every 2 h, $x(t)$ and $w(t)$ are used to develop and refine deterministic strategic-level flow control initiatives, which, for the purpose of this initial study, consist of assigning predeparture delays to flights subject to airport and airspace capacity constraints. The high-level steps associated with this process are depicted by the three boxes that are labeled "Strategic Departure Control Model," "Strategic Demand Estimation," and "Strategic Weather Translation" in Fig. 1. The first step in developing these strategic-level controls is to convert the weather data $w(t)$ into reduced-sector-capacity estimates, which is accomplished by the strategic weather translation module. The weather translation model adopted is described in Secs. III.C and III.D. Subsequently, the predicted positions of all airborne and scheduled flights over a user-defined planning horizon is calculated by the strategic demand estimation module. This strategic demand estimation system was also chosen to be a version of FACET for this study. The planning horizon used and the frequency at which the strategic-level model was called are discussed in Sec. III.A. The forecasted system demand and capacity estimates are used as inputs to the strategic departure control model module. A description of this model is provided in Sec. II.B. The controls generated by this model, $u^{\text{depart}}(t)$, are flight-specific predeparture delays that are subsequently passed to the primary simulation for implementation.

Refinements to the strategic-level traffic flow management plan to account for uncertainties in the demand and capacity estimates are accomplished through two tactical control loops. The first of these tactical control loops (depicted by the three boxes labeled "Tactical Weather Translation," "Trajectory Intersects Weather Check," and "Deterministic Weather Rerouting" in Fig. 1) is called at a frequency that ranges between 5 and 30 min, and it assigns tactical reroutes to flights to ensure that aircraft do not venture into significant convective weather. The variable calling frequency is allowed here to account for the confidence in the weather forecast accuracy, and the impact of varying this parameter is explored in detail in Sec. IV.B. These regions of significant convective weather are defined by the tactical weather translation module, which is described in more detail

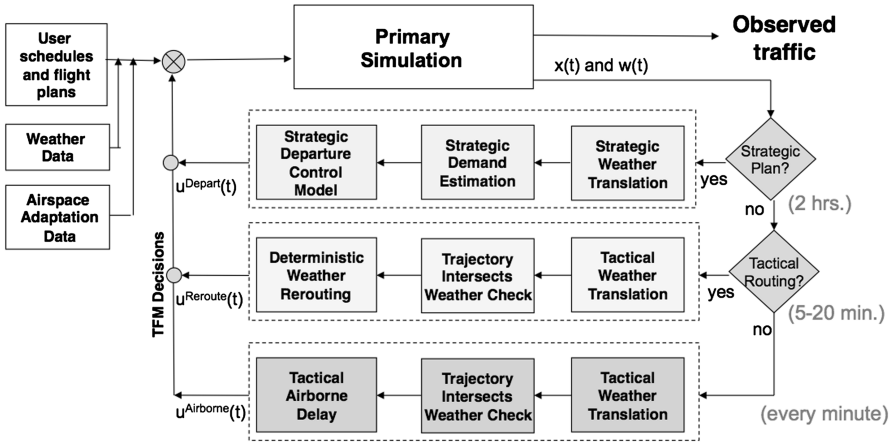

Fig. 1 Integrated optimization-simulation architecture.

in Sec. III.D. The trajectories of all flights over a 100 to 400 n mile look-ahead horizon are checked to determine if any flight intersects one of the identified regions of significant convective weather in the trajectory-intersects weather-check module. Flights found to intersect these regions are subsequently rerouted in the deterministic weather rerouting module, using the algorithm described in Sec. II.C. The tactical aircraft-level rerouting controls $u^{\text{reroute}}(t)$ are subsequently passed back into the primary simulation for implementation.

The lowest-level control loop that is called every minute is used as a control strategy of last resort to immediately assign airborne delay to any flight that will encounter an en route weather hazard within the next minute. These controls are labeled as $u^{\text{airborne}}(t)$ in Fig. 1. The en route weather hazards being avoided are defined by the tactical weather translation module and will be described in Sec. III.D. The three high-level steps associated with this process are depicted by the three boxes labeled "Tactical Weather Translation," "Trajectory Intersects Weather Check," and "Tactical Airborne Delay" in Fig. 1. A description of the tactical airborne-delay algorithm is presented in Sec. II.D.

B. Departure Control Model

The parameters for the binary integer programming model that was used to assign departure delays are defined in this section. Note that the definition of x and w in this section differ from the definitions of these variables in the previous section.

The binary decision variables in the model, $x_{f,t} \in \{0, 1\}$, are defined as

$$x_{f,t} = \begin{cases} 1 & \text{if flight } f \text{ departs by time } t \\ 0 & \text{otherwise} \end{cases} \tag{1}$$

Based on the decision variables $x_{f,t}$, a set of auxiliary variables, $w^j_{f,t} \in \{0, 1\}$, which indicates if a flight f has entered sector j, where $j = P(f, i)$, $1 < i < N_f$ by time t, is defined as

$$w^j_{f,t} = x_{f,t-\sum_{m=1}^{i-1} l_{f,P(f,m)}} \tag{2}$$

With this definition of $x_{f,t}$, the objective of this model is to minimize the total ground delay with respect to the unconstrained schedule, and is expressed as

$$\min \sum_{f \in F} \sum_{t=d_f}^{d_f+G} (t - d_f)(x_{f,t} - x_{f,t-1}) \tag{3}$$

The set of constraints is described as follows:

Airport departure capacity is the number of departures from an airport k during any time period that are bounded by airport departure capacity:

$$\sum_{f:\ P(f,1)=k} (x_{f,t} - x_{f,t-1}) \le D_k(t) \quad \forall\ k \in K, \qquad t \in \{1, \ldots, T\} \tag{4}$$

Airport arrival capacity is the number of landings during any time interval that are limited by airport arrival capacity:

$$\sum_{f:\ P(f,N_f)=k} (x_{f,t} - x_{f,t-1}) \le A_k(t) \quad \forall\ k \in K, \qquad t \in \{1, \ldots, T\} \tag{5}$$

Sector capacity ensures that the number of aircraft present in sector j at time t does not exceed the sector capacity:

$$\sum_{\{f:\ j=P(f,i),\, j'=P(f,i+1),\, i<N_f\}} (w^j_{f,t} - w^{j'}_{f,t}) \le S_j(t) \ \ \forall\, j \in J, \quad t \in \{1, \ldots, T\} \tag{6}$$

The baseline sector capacities $S_j(t)$ were taken to be the monitor-alert parameters (MAP). However, only a subset of all flights in the region of airspace considered was subject to predeparture delays, which is discussed in Sec. III.C. This was done solely to improve runtime performance. To account for the impact of these uncontrolled flights on the sector capacities, the time-varying demand associated with these flights was calculated and subtracted from the nominal sector MAP to provide an estimate of the actual capacity available in each sector. Furthermore, the strategic weather translation module that is illustrated in Fig. 1 and described in Sec. III.D was used to further reduce the values of $S_j(t)$ to account for en route weather impacts.

Time connectivity requires that the decision variables are monotonically increasing:

$$x_{f,t} - x_{f,t-1} \ge 0 \quad \forall\ f \in F, \qquad t \in \{d_f, \ldots, d_f + G\} \tag{7}$$

The maximum allowed departure delay is

$$x_{f,d_f+G} = 1$$

Note that the original model presented in [8] also includes a set of flight connectivity constraints. Because these constraints were not relevant to the current en route flight scheduling problem, their description has been omitted. Additionally, the extra variables and constraints that allowed airborne delay to be assigned to individual flights in the original model have been removed and airborne delay is assigned independently, using the model presented in II.D. By decoupling the assignment of predeparture delays and airborne delays to flights, the current approach can more readily assign airborne delay to flights in response to changing weather conditions. An added benefit of this decoupling is that the runtime performance of the current model has also been greatly improved. Finally, the integer constraint on $x_{f,t}$ was relaxed to enhance the solvability of this model. The strong formulation of this model resulted in $x_{f,t}$ taking on values of only 0 or 1 for the test cases examined in this study.

C. Deterministic Weather Rerouting Model

The rerouting of individual flights and flows of traffic in the presence of either deterministic or probabilistic weather hazards is a rich area of research [15–17]. Flight-specific weather-avoidance routes for this study were calculated using Dijkstra's algorithm [12] to solve the shortest-path problem on a weighted directed graph $G = (V, E)$. This approach led to a factor-of-30 reduction in the computational runtime over the rerouting model used in [10] that relied on a linear-programming-based shortest-path algorithm.

The set of vertices V was generated by uniformly distributing 60 latitude points and 60 longitude points within the polygon defined by 43° latitude to the north, 29° latitude to the south, −93° longitude to the west, and −70° longitude to the east. This region and the corresponding routing nodes are illustrated in Fig. 2, along with the

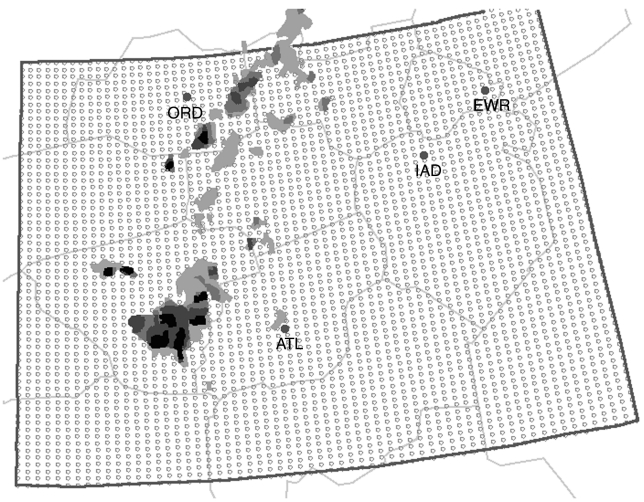

Fig. 2 Flight control region (dark-gray polygon) and tactical routing grid (gray circles) with the CWAM 20, 40, 60, and 80% deviation probability contours at 30,000 ft at 1200 hrs UTC on 19 June 2007.

CWAM 20, 40, 60, and 80% deviation probability contours at 30,000 ft at 1200 hrs UTC on 19 June 2007. With these parameters, a routing grid in which the horizontal and vertical distance between adjacent nodes was approximately 17 n mile was generated that encompassed most of the eastern region of the United States.

The set of all edges E connecting the routing nodes was generated by connecting each point to its eight nearest neighbors, and the cost of traversing each edge was calculated. For this study, the cost was nominally set to the great circle distance connecting the two nodes forming a particular edge. Each edge that intersected a weather hazard was subsequently weighted by a large penalty factor, which was set to a value of 1000.

An example of a tactical weather-avoidance reroute for a flight that was nominally scheduled to travel from Chicago O'Hare (ORD) airport to Newark International (EWR) airport on the flight path illustrated by the solid black line is shown in Fig. 3. The rerouted portion of the flight path, which is depicted by the dashed gray line, is generated from the starting node i_1 to the ending node i_N, and this rerouted flight-path segment is subsequently reinserted into the original scheduled route to generate the weather-avoidance route. For reference, this reroute was generated to avoid the CWAM 60% deviation probability contours at 30,000 ft, which are depicted by the solid gray polygons in Fig. 3.

D. Tactical Airborne Delay

A 1 min dead-reckoning trajectory is generated for each aircraft and is used in the trajectory-intersects weather-check module that is illustrated in Fig. 1, to identify flights requiring tactical airborne delay. In general, tactical airborne delay can be achieved by controls such as circular holding, path stretching, or speed control. For this study, tactical airborne delay was achieved through circular holding. Flights requiring tactical airborne delay are those flights for which neither a predeparture delay nor a deterministic reroute could be generated to ensure that the flight did not deviate into a weather hazard. A number of factors can contribute to flights receiving airborne delay, such as having a weather hazard located directly over the arrival or departure airport. Additionally, the 50 n mile grid used for the rerouting algorithm (see Sec. II.C) is often too coarse to generate a reroute that avoids the en route weather hazards, but reducing this grid spacing can significantly increase the runtime of the rerouting algorithm.

When determining if a flight was a candidate for airborne delay, the line segment formed by connecting the aircraft's current position with this forecasted position was compared against all line segments forming the contours of the weather hazards. If this segment intersected a weather hazard, then the tactical airborne delay module that is depicted in Fig. 1 assigned 1 min of airborne delay to the flight in the primary simulation. For reference, the dead-reckoning trajectory is generated with the assumption that an aircraft will maintain its current course, airspeed, and altitude over the next minute. A secondary simulation could have been used to generate this trajectory, but the computational overhead associated with launching this system every minute was not warranted.

III. Experimental Setup

The frequency at which the strategic and tactical flight control models were called, the set of potentially controlled flights, and the weather translation models used are described in this section. For all experimental runs, the unscheduled flight demand set was derived from the 24 August 2005 ETMS data set. The ETMS data parsing logic in FACET extracted the following messages to generate the inputs for the fast-time simulations: departure messages (DZ), flow control track/flight data block messages (TZ), and flight plan messages (FZ). The TZ messages were used to establish an initial position for each flight, the FZ messages were used to assign baseline flight paths to each flight, and the DZ messages were used to establish departure times.

A. Planning Intervals

All fast-time experimental results assumed a start time of 1000 hrs Coordinated Universal Time (UTC), which corresponds to 0600 hrs Eastern Daylight Time (EDT), and a 6 h planning horizon, as illustrated in Fig. 4. Every 2 h, starting at 1000 hrs UTC, the strategic departure control model illustrated in Figs. 1 and 4 was solved for a 2 h planning horizon, and the departure controls were applied to the primary simulation shown in Fig. 1. In follow-up studies, the effect of varying the duration and frequency of this strategic-planning phase will be explored.

The tactical rerouting controls labeled in Figs. 1 and 4 were nominally calculated once every 5 min using the methodology described in Sec. II.C. To explore the sensitivity of these reroutes to the planning interval, subsequent fast-time simulations were conducted for which rerouting occurred at frequencies of 10, 15, and 20 min. These results are presented in Sec. IV. Finally, the tactical airborne-delay controls labeled in Figs. 1 and 4, were applied every minute, using the method described in Sec. II.A.

B. Tactically Controlled Flights

The set of flights that were candidates for either tactical rerouting or airborne delay consisted of all flights that resided within the gray polygon depicted in Fig. 2. This region includes all or most flights in the following centers: Chicago; Cleveland; Boston; New York; Indianapolis; Washington, D.C.; Memphis; Kansas City; Fort Worth; Jacksonville; and Atlanta. The time-varying count of flights subjected to tactical flight controls for the 24 August 2005 data set is shown in Fig. 5. The minimum number of potentially controllable flights was 530, which occurred at 1000 hrs UTC, and the maximum

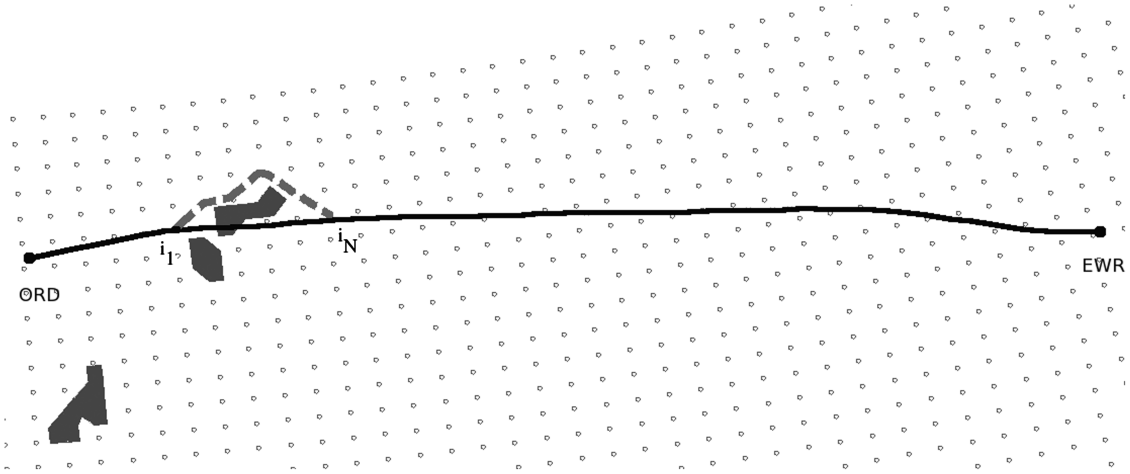

Fig. 3 Nominally scheduled route (solid black line) for a flight between Chicago O'Hare (ORD) and Newark International (EWR) and tactical reroute (dashed gray line) that avoids the CWAM 60% deviation probability contours at 30,000 ft (gray polygons).

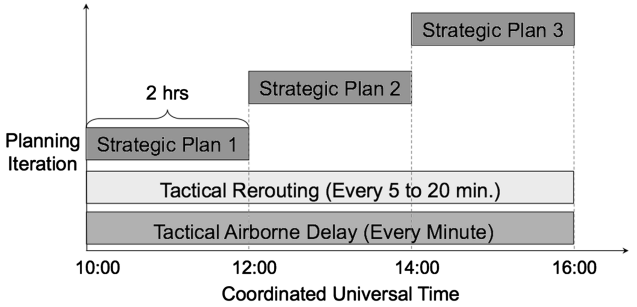

Fig. 4 Strategic and tactical flight control planning frequency versus time.

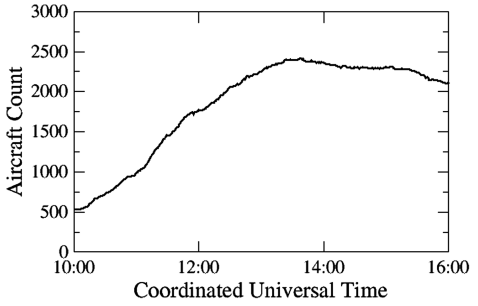

Fig. 5 Time-varying count of aircraft subject to tactical flight controls.

instantaneous number of controllable flights was 2412 at 1337 hrs UTC.

C. Strategic Model Flights and Constraints

For the strategic departure control model that was described in Sec. II.B, all predeparture flights that were nominally scheduled to depart from one of the following centers at any time during the 2 h strategic-planning horizon were candidates for departure control: Chicago; New York; Cleveland; Indianapolis; Washington, D.C.; Fort Worth; Atlanta; Memphis; Jacksonville; and Kansas City. The sole reason for not including all flights in the departure control model was to improve the runtime performance of this model. In future studies, more sophisticated techniques, such as the congestion score approach developed in [18], will be used for identifying flights to include in the model. Collectively, the airspace of these 10 centers generally cover the polygon illustrated in Fig. 2. Using the 24 August 2005 data set, 2701 flights were included in the first call to the strategic departure control model that covered the period from

Fig. 6 Graphical illustration of the airspace constraints included in the strategic departure control model.

1000 to 1200 hrs UTC (see Fig. 4), 4576 flights were included in the second call to this model that started at 1200 hrs UTC and extended to 1400 hrs UTC, and 4283 flights were included in the third call that started at 1400 hrs UTC and extended to 1600 hrs UTC.

The geographical distribution of the airspace constraints appearing in Eqs. (4–6) is illustrated in Fig. 6. The 949 gray squares represent the location of the airport arrival and departure capacity constraints appearing in Eqs. (4) and (5), and the gray highlighted sectors depict those sectors for which capacity constraints were included in Eq. (6). Note that the current problem formulation contains constraints for 987 sectors, but only the location of the high-altitude sector-capacity constraints are illustrated in Fig. 6. This set of airspace constraints was constructed by identifying the set of all unique arrival airports, departure airports, and sectors that the aforementioned set of flights was nominally schedule to fly through.

The airport arrival and departure capacities were set to the nominal rates for each of these airports as defined in the ETMS system, in which, for example, the nominal departure rate for EWR is 15 aircraft per 15 min and the airport arrival rate is 10 aircraft per 15 min. As discussed in the previous section, the nominal sector capacities were set to the monitor-alert parameter for each sector and were subsequently reduced to account for the impacts of en route convective weather, which will be discussed in the next subsection, and the time-varying background demand of flights that were not candidates for predeparture delays. An example of the original monitor-alert value for sector 47 in the Chicago center is illustrated by a solid black line in Fig. 7a, and the reduced capacity that accounts for the uncontrolled time-varying traffic demand is depicted by a dashed gray line. For reference, the Chicago center boundary, the high-altitude sectors in this center, and the regions with CWAM 60% deviation probability contours at 30,000 ft are depicted in Fig. 7b. The highlighted sector in this figure is sector 47.

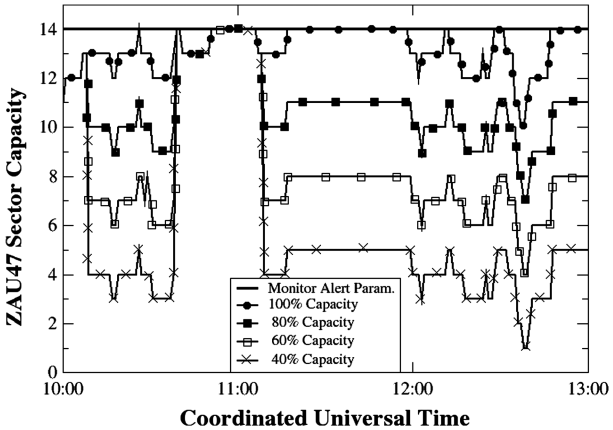

a)

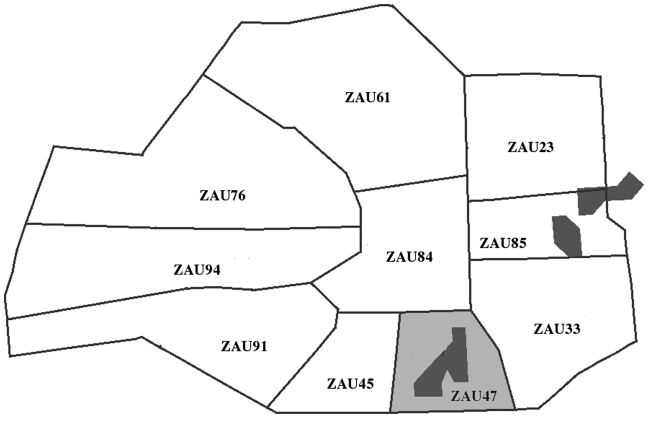

b)

Fig. 7 Impact of CWAM 60% deviation probability contours at 30,000 ft shown on a) the sector capacity of Chicago sector 47 (ZAU47) between 1000 and 1300 hrs UTC and b) sector 47 (highlighted) in Chicago center at 1130 hrs UTC.

D. Weather Constraints

The weather scenario used was developed using actual and forecasted CWAM deviation probability contours [13] from 19 June 2007. For reference, CWAM provides aircraft deviation probability contours over a 2 h planning horizon in 5 min increments and is updated every 5 min. These contours are calculated between 24,000 and 44,000 ft in 1000 ft increments, with deviation probabilities that range from 0 to 100%. The convective weather on this day consisted of a squall line that extended from the United States–Canada border into Memphis center by early morning (see Fig. 2). This line of storms moved in an easterly direction throughout the day and impacted much of the eastern shoreline by midafternoon. This weather pattern resulted in widespread delays throughout the NAS, based on statistics available through the FAA's Operations Network [19] database. For reference, 207,912 min of delay were logged on this day. In contrast, only 19,712 min of delay were recorded for 24 July 2007, which can be described as a good weather day.

As noted in Fig. 1, the influence of weather on the air traffic was captured through two independent mechanisms. For strategic planning, the box in Fig. 1 labeled "Strategic Weather Translation" was used to calculate weather-impacted sector capacities that were used in Eq. (6) of the departure control model. For this initial study, a simple weather translation model was used that reduced the nominal sector capacities, which were taken to be the monitor-alert parameters, by fixed percentages (i.e., 0, 20, 40, and 60%) if any portion of a sector was impacted by a CWAM 60% deviation probability contour, which denotes a region of airspace that 60% of all flights are likely to avoid, at 30,000 ft. This is acknowledged to be a simplistic model that will be refined in the future to leverage the state of the art in weather translation modeling [20–26].

An example of the weather-impacted sector capacities for sector 47 in Chicago center as a function of time between 1000 and 1300 hrs UTC is shown in Fig. 7a. For reference, this sector is depicted by the gray filled polygon in Fig. 7b. The solid line represents the MAP, which was used as the nominal sector capacity; the line with filled circles represents the residual capacity when accounting for the time-varying demand of the flights not controlled by the departure control model; the line with filled squares represents the residual capacity when weather results in a 20% reduction in capacity; the line with open squares represents the capacity when the impact of weather is to reduce the capacity by 40%; and the line with crosses represents the capacity when weather results in a 60% reduction in the sector capacity. For reference, the location of the CWAM 60% probability deviation contours that were present at 30,000 ft at 1200 hrs UTC is illustrated in Fig. 7b.

For the tactical flight controls (e.g., rerouting and airborne delay), the regions of airspace that flights were to avoid due to convective weather were defined to be the CWAM 60% deviation probability contours at 30,000 ft. This is admittedly a simplification, because the altitude-varying deviation probabilities are not being explicitly taken into account, but, as will be seen in Sec. IV.C, reroutes generated with these weather-avoidance polygons were in good agreement with the reroutes actually flown on 19 June 2007. For airborne delay, only the current CWAM observations (i.e., 0 min forecasts) were used. However, for tactical rerouting, the current observations as well as the 5, 10, 15, 20, 25, and 30 min forecasts were used to construct a three-dimensional grid (i.e., latitude, longitude, and time) for assigning the costs to the edges used in the shortest-path rerouting algorithm. Follow-up studies that explore the use of CWAM forecasts up to 2 h would be beneficial.

IV. Results

This section contains the results of 32 six-hour fast-time simulation experiments to study the ability of the optimization-simulation approach to assign strategic predeparture delays, tactical reroutes, and airborne delay to flights subject to the airport and airspace capacity constraints described in Sec. III. It should be stressed that these simulations were conducted solely for the purpose of testing this new approach, and the results are likely to be highly dependent on the weather scenario being considered. To limit the size of the test matrix, the sensitivity of the total delays, the weighted total delay cost, airborne delays, rerouting delays, and ground-holding delays were examined in terms of variations in the rerouting look-ahead distance, the rerouting frequency, and the available capacity of the weather-impacted sectors. Additionally, this section also contains the results of an initial attempt to validate the results of the weather-avoidance rerouting algorithm. Throughout this section, no attempt was made to use a consistent set of vertical-axis limits, although Figs. 8–13 all contain plots of delays. The primary reason for doing so is because of the vast differences in the magnitudes of some of these delays.

A. Sector Capacity Versus Rerouting Look-Ahead Distance

Plots of the total delays, the total weighted delay cost as a function of the rerouting look-ahead distance, and the percent reduction in the weather-impacted sector capacities are presented in Figs. 8a and 8b, respectively. Here, the weighted delay cost is equal to the sum of the ground delays, the rerouting delays weighted by a factor of 2, and the airborne delays weighted by a factor of 30. The factor-of-2 weighting for the rerouting delays is justified based on the increased cost of fuel consumption for a flight on the ground versus in the air. The factor-of-30 weighting associated with the airborne delay accounts for this increased fuel consumption cost, as well as an additional penalty factor, because tactical airborne delays can greatly increase the complexity of a region of airspace [27]. The factor of 30 was selected based on engineering judgment, and follow-up research

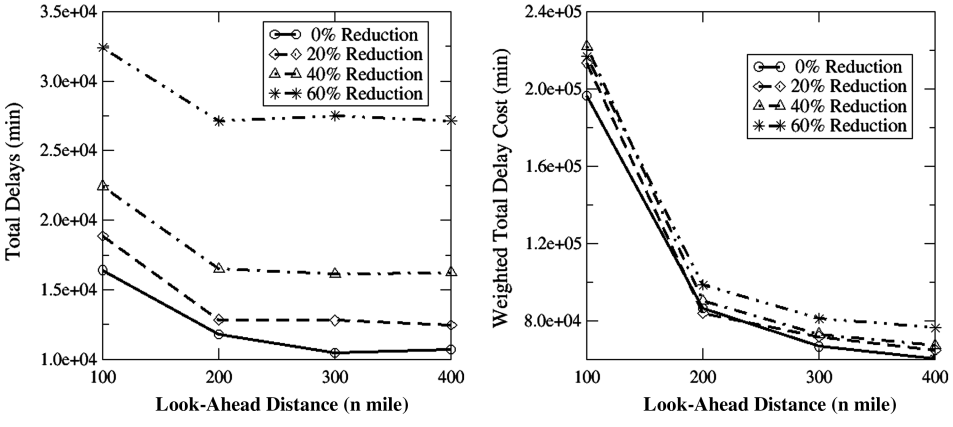

Fig. 8 Impact of rerouting look-ahead distance and reduction in the weather-impacted sector capacity on a) the total delays and b) a weighted sum of the ground delays, rerouting delays, and airborne delays. Sector capacity reduced from 0 to 60% in 20% increments, and look-ahead distance varied from 100 to 400 n mile in 100 n mile increments.

that explicitly quantifies the added cost of airborne holding over ground holding is needed. Finally, all results in this subsection assume that an aircraft for which the flight path is forecasted to intersect a CWAM weather contour can be rerouted every 5 min, which corresponds to the CWAM weather update rate.

Interesting trends are apparent from the total delay curves in Fig. 8a. The most notable trend is that the total delay is only moderately sensitive to minor reductions (e.g., $\leq 40\%$ capacity reductions) in the capacities of the weather-impacted sector capacities that appear in Eq. (6); however, the total delays increase rapidly as the perceived impact of the weather on the sector capacities approaches a 60% reduction. This would imply that under nominal conditions, few of the 987 sector capacities (see Sec. III.C) appearing in Eq. (6) are binding constraints, but as the perceived impact of weather on the sectors' capacities worsens, more of the constraints appearing in Eq. (6) become binding, leading to higher total delays. The results in Fig. 8a also exhibit a general trend in which higher delays are observed for very short rerouting look-ahead distances (e.g., 100 n mile). As will be seen later in this section, these very short look-ahead distances are associated with very myopic reroutes with considerable airborne delays. Note that the total delays in Fig. 8a are, in some cases, nearly an order of magnitude smaller than the total delays reported in [10]. These delay reductions are largely due to the improved weather translation model currently being used (see Sec. III.D) and, to a lesser extent, to the reduction in the spacing between adjacent nodes in the rerouting grid. When a weighting factor of 2 is applied to the rerouting delays and a factor of 30 is applied to the airborne delays, then the weighted total delay costs that are shown in Fig. 8b for the four alternative weather-impacted sector-capacity scenarios yield nearly identical results in terms of overall cost. In all cases, the weighted total delay cost increases rapidly with shorter rerouting look-ahead distances, for which costly airborne delays become more prevalent.

The airborne-delay and ground-holding-delay results shown in Figs. 9a and 9b, respectively, exhibit a number of interesting trends. First, the airborne delays are greatest for short look-ahead distances, and the amount of airborne delay is roughly independent of the amount by which the weather-impacted sector capacities appearing in Eq. (6) are reduced. Note that a considerable amount of the airborne holding is associated with flights that either depart from or arrive at an airport that is impacted by convective weather. In these cases, the rerouting algorithm is simply incapable of generating an alternative reroute for avoiding the weather. In regard to the ground delays, small reductions in the sector capacities have minimal effect on the ground delays, but these delays increase rapidly as the reductions in the weather-impacted sector capacities increase, because more of the constraints in Eq. (6) become binding under these circumstances. Another interesting trend is that the ground delays are, for the most part, independent of the rerouting look-ahead distance, which will be discussed in more detail subsequently.

The rerouting delays and the number of reroutes are presented in Fig. 10. The rerouting delays were found to decrease rapidly with increasing rerouting look-ahead distance, but the number of reroutes tended to increase with increasing rerouting look-ahead distance. This increase in the number of reroutes with large look-ahead distances is expected, because only CWAM forecasts up to 30 min

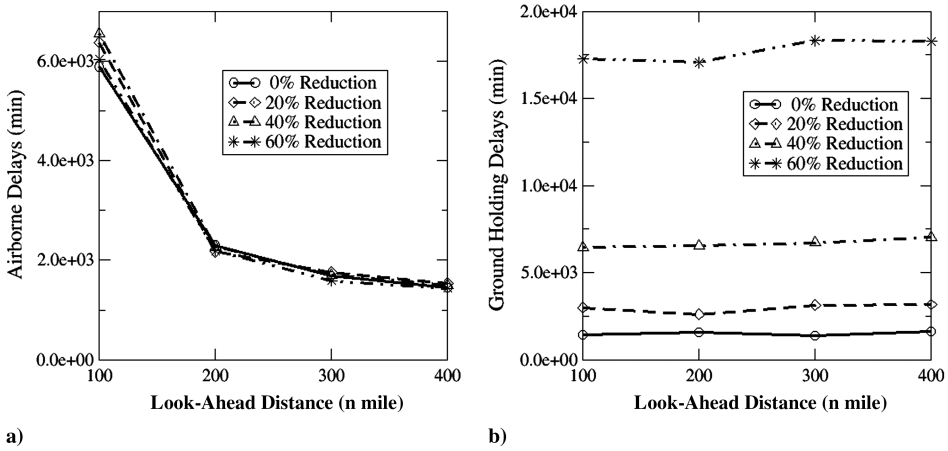

Fig. 9 Impact of rerouting look-ahead distance and reduction in the weather-impacted sector capacity on a) the airborne delays and b) the ground-holding delays. Sector capacity reduced from 0 to 60% in 20% increments, and look-ahead distance varied from 100 to 400 n mile in 100 n mile increments.

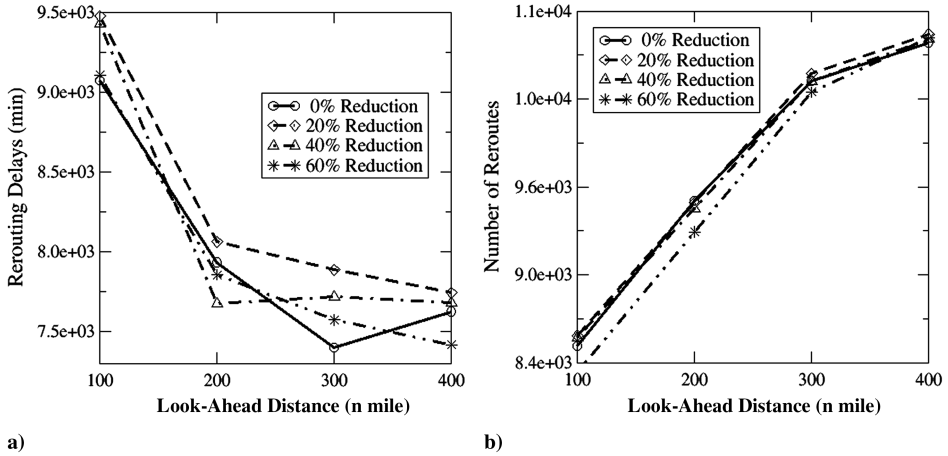

Fig. 10 Impact of rerouting look-ahead distance and reduction in the weather-impacted sector capacity on a) the rerouting delays and b) the number of reroutes. Sector capacity reduced from 0 to 60% in 20% increments, and look-ahead distance varied from 100 to 400 n mile in 100 n mile increments.

were considered, yet forecasts valid up to 1 h are ideally required when generating a reroute with a 400 n mile look-ahead distance. For very short look-ahead distances, myopic and aggressive reroutes were being generated that tended to cause significant deviations from the nominally schedule flight paths, but fewer of these tactical reroutes were required. Follow-up studies that explore the utility of using CWAM forecasts up to 2 h under a variety of weather scenarios would be beneficial. Note that the rerouting delays in Fig. 10a are nearly an order of magnitude smaller than the rerouting delays reported in [10]. This significant reduction in delays is primarily due to the improved tactical weather translation model that is being used that leverages the CWAM model (see Sec. III.D).

Finally, the rerouting delays and the number of reroutes were found to be nearly independent of the severity of the weather-affected sector-capacity constraints being considered in Eq. (6), as illustrated in Fig. 10b. This is a significant finding and illustrates a basic disconnect between the way in which weather is being accounted for in the strategic departure control model and the tactical rerouting model. At the root of this problem is the manner in which weather impacts are accounted for in the strategic departure control model. Rather than identifying and controlling individual flights or flows that are predicted to be impacted by weather hazards, any flight passing through a weather-impacted sector can potentially be subject to a predeparture delay, regardless of whether it will actually be impacted by the weather. This point warrants follow-up studies, because this problem impacts not only the model being used in this study, but also the model proposed in the seminal work of [7].

B. Rerouting Frequency Versus Rerouting Look-Ahead Distance

Figure 11 contains plots of the total delays and the total weighted delay cost as a function of the rerouting look-ahead distance and the frequency at which new reroutes can be created. All results in Figs. 11–13 were calculated using the sector capacities in Eq. (6), in which the nominal MAP values (i.e., the 0% capacity reduction scenario) have been reduced by the time-varying demand of the uncontrolled traffic (i.e., the 100%-available-sector-capacity case), which was described in Sec. III.C. Therefore, the tactical rerouting algorithm and the airborne-delay model are responsible for keeping flights from deviating into weather hazards, and the strategic departure control model is solely responsible for resolving volumetric constraints (i.e., too many flights arriving in a sector, departing from an airport, or arriving at an airport at any instant of time).

When ground, airborne, and rerouting delays are assumed to have equal costs, the total delays in Fig. 11a are found to decrease with increasing rerouting look-ahead distances and, to a lesser extent, with increasing rerouting frequency. However, when the frequency at which flights are rerouted approaches 20 min, the delays tend to noticeably increase because of the increased need for airborne holding. Alternatively, when the cost of each of these delay types is weighted differently, the weighted total delay costs in Fig. 11b exhibit very clear trends in which the delay costs increase as the frequency at which flights are rerouted increase. The significant cost associated with airborne holding, which is more prevalent when the rerouting frequency decreases, is primarily responsible for this trend,

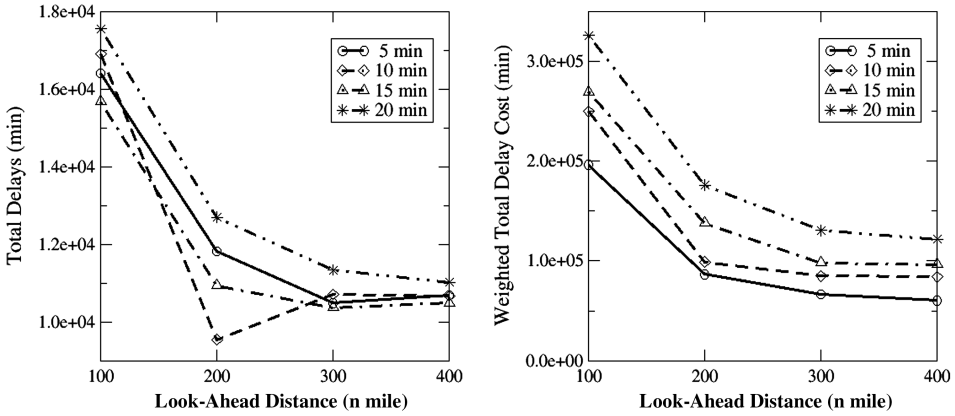

Fig. 11 Impact of rerouting look-ahead distance and rerouting frequency on a) the total delays and b) a weighted sum of the ground delays, rerouting delays, and airborne delays. Rerouting frequency varied from 5 to 20 min in 5 min increments, and look-ahead distance varied from 100 to 400 n mile in 100 n mile increments.

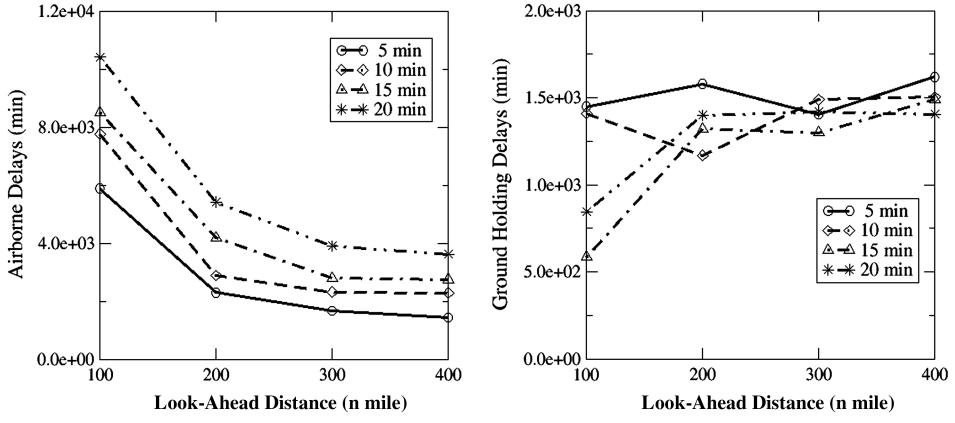

Fig. 12 Impact of rerouting look-ahead distance and rerouting frequency on a) the airborne delays and b) the ground-holding delays. Rerouting frequency varied from 5 to 20 min in 5 min increments, and look-ahead distance varied from 100 to 400 n mile in 100 n mile increments.

because with a higher rerouting frequency, flights are able to find gaps through the weather without relying on costly airborne delays.

The airborne delays and ground-holding delays are illustrated in Figs. 12a and 12b, respectively. As previously noted, the airborne delays increase rapidly as the frequency at which flights are rerouted decreases. Additionally, airborne delays are highest with shorter rerouting look-ahead distances, for which the algorithm is attempting to generate tactical weather-avoidance reroutes on a routing grid on which grid points are separated by approximately 17 n mile. Decreasing the rerouting grid spacing would allow the algorithm to perform better at the short look-ahead distances, but would increase the runtime performance of the rerouting algorithm. In terms of the ground-holding delays that are shown in Fig. 12b, the delays are found to be insensitive to the frequency at which flights are rerouted when the rerouting look-ahead distance is $\geq$ 200 n mile, and because few of the 987 sector-capacity constraints (see Sec. III.C) appearing in Eq. (6) are binding in these scenarios, the delays are relatively small.

Figure 13 contains plots of the total rerouting delays and the number of reroutes as a function of the rerouting frequency and the rerouting look-ahead distance. In general, the number of delays and reroutes decrease with decreasing rerouting frequency, but this is not an indication that the routing is working well in this area; in fact, the opposite is true. When the rerouting frequency is greater than 15 min, the rerouting algorithm becomes increasingly less effective at avoiding the weather hazards, causing the airborne delays to greatly increase. In terms of rerouting look-ahead distance, the delays are worse for short look-ahead distances (i.e., 100 n mile) for which myopic reroutes are being created, and delays tend to decrease with increasing look-ahead distance. The latter observation is likely dependent on the type of weather encountered. It may not hold true for less structured weather cells or for cells that are rapidly growing or decaying. Finally, it is interesting to note that the highest level of rerouting controls occur with a 400 n mile look-ahead distance and a rerouting frequency of 5 min. In this case, strategic reroutes are being developed, but are being fine-tuned at a high frequency to adapt to weather hazards that a flight may or may not encounter after nearly an hour of travel time. For these longer routing look-ahead distances, less frequent rerouting update rates on the order of 10 to 15 min are more appropriate. Overall, the rerouting algorithm performs reasonably well over a look-ahead distance of 200 to 400 n mile when rerouting occurs at a frequency of 5 to 15 min. Future testing of the algorithm on a larger range of weather scenarios would be beneficial.

C. Model Validation

An important issue to consider when developing and testing any new modeling capability is the accuracy of the estimated impact metrics. The integrated optimization-simulation model developed in support of this study assigns ground-holding, rerouting, and airborne delays to individual flights to keep these flights from deviating into weather-impacted regions of the NAS. Ideally, a validation of this model would entail a direct comparison between the model-generated controls and, for example, the controls used in current-day air traffic operations. As a first step, this section provides the results of an initial validation of the rerouting algorithm, which emerged as the primary control strategy for ensuring that aircraft avoid regions of en route convective weather.

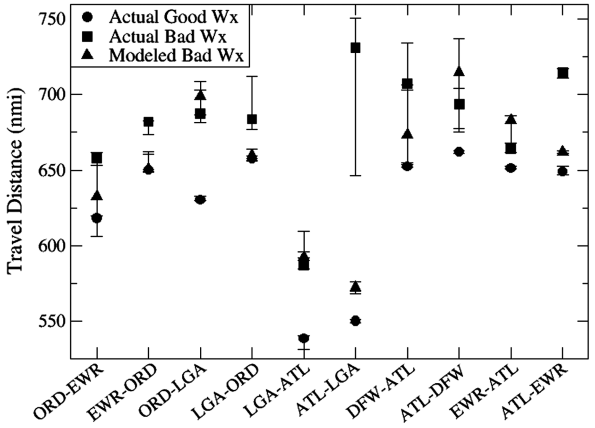

Fig. 14 Actual observed travel distances between 10 city pairs on a good weather day (solid circles), actual observed travel distances on a bad weather day (solid squares), and modeled travel distances on a bad weather day (solid triangles).

To perform this validation, the flight-path distances between all major origin and destination pairs in the eastern region of the United States were calculated under three scenarios. Under scenario 1, the actual travel distances on a good weather baseline day, which was taken to be 24 August 2005, were calculated from the ETMS position messages (TZ). For scenario 2, the actual travel distances on a bad weather day, which was taken to be 19 June 2007, were calculated from the ETMS position messages. Finally, the rerouting model described in Sec. II.C was used with the tactical weather translation model described in Sec. II.D to calculate the travel distances for all flights nominally scheduled on 24 August 2005, using the weather data from 19 June 2007. A comparison of these three travel distances for 10 of the origin-destination pairs considered in support of this validation exercise is shown in Fig. 14. For data presentation purposes, travel distances between a given origin and destination pair (for example, ORD and EWR) were arranged in numerical order and separated into quartiles. The data symbols in Fig. 14 were placed at the median of each data set; the lower limits of the error bars were positioned at the first quartile, or the median of the lower part of the data; and the upper limits of the error bars were positioned at the third quartile, or the median of the upper part of the data.

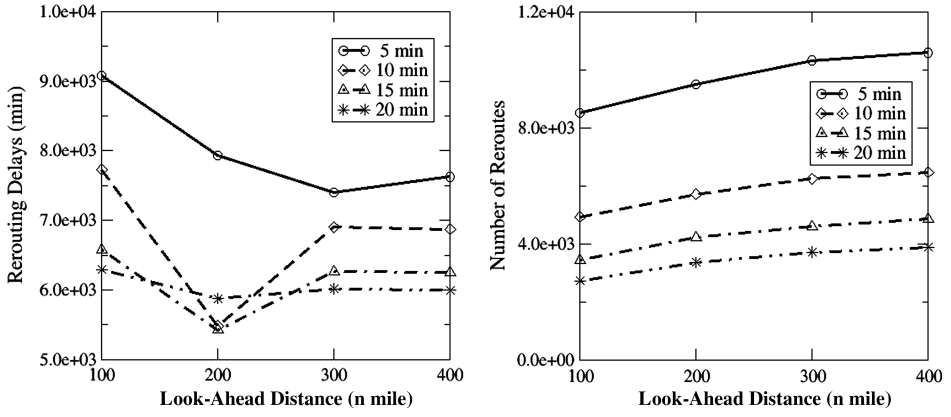

Fig. 13 Impact of rerouting look-ahead distance and rerouting frequency on a) the rerouting delays and b) the number of reroutes. Rerouting frequency varied from 5 to 20 min in 5 min increments, and look-ahead distance varied from 100 to 400 n mile in 100 n mile increments.

From the data presented in Fig. 14, a number of interesting trends emerge. First, the actual travel distances on the good weather day (solid circles) are always the shortest, which is to be expected. Second, the actual observed travel distances on the bad weather day (solid squares) are typically the longest. Finally, the modeled predicted travel distances for the bad weather day (solid triangles) typically reside between the actual good weather distances and the actual bad weather distances. These results are consistent with the travel distances that were observed for all other major origin and destination pairs that were examined, and these results indicated the following:

1) The rerouting algorithm is working correctly.

2) The tactical weather translation model is correctly identifying those regions of airspace that flights typically avoid.

The few cases in which the mean travel distances for the modeled reroutes are longer than the distances that were actually observed on the bad weather day are the results of overestimating the impact of the convective weather. Examples of these cases include the travel distances between ORD and LaGuardia Airport (LGA) (ORD-LGA), Atlanta International Airport (ATL) and Dallas/Fort Worth International Airport (DFW) (ATL-DFW), and EWR-ATL. Modifying the rerouting algorithm to explicitly account for the altitude-varying CWAM deviation probabilities is expected to correct this trend.

V. Conclusions

This paper proposes an innovative sequential optimization approach for generating traffic flow management controls in the presence of uncertain flight intent and weather information and an integrated optimization-simulation framework for testing this approach, and it tests this approach by conducting 32 six-hour fast-time simulation experiments. The weather-impacted traffic scenario used was derived from operational enhanced traffic management system flight data from 24 August 2005 and the convective-weather-avoidance model deviation probability contours from 19 June 2006. This weather day was selected because of the severity and intensity of the squall line that extended from the United States–Canada border to the southern portion of the United States.

The experiments examined variations in the ground-holding, rerouting, and airborne delays and controls in terms of variations in the rerouting look-ahead distance, the rerouting frequency, and the available capacity of the weather-impacted sectors. The experimental results highlighted a fundamental difference in the way in which weather impacts were being considered with the tactical rerouting and airborne-delay controls and the manner in which these constraints were accounted for in the strategic departure control model. Although the tactical controls were explicitly taking into account the impact of weather hazards on individual flights, the departure control model was accounting for these constraints in a more aggregate sense by translating the impacts of weather into changes in the sector-capacity constraints. The benefits of the strategic departure control model were therefore limited because of the lack of consistency in the strategic and tactical weather translation models. Follow-up studies that explore techniques for explicitly accounting for the impact of weather hazards on individual flights or flows within a strategic traffic flow model are required to resolve this discrepancy.

Finally, an initial validation of the rerouting algorithm was undertaken, which emerged as the primary control strategy for ensuring that aircraft avoid regions of en route convective weather. The results of this validation indicate that the algorithm is able to generate reroutes that are, on average, shorter than operationally flown weather-avoidance routes when regions of airspace that flights are likely to avoid are identified using the convective-weather-avoidance model.

Acknowledgment

The authors would like to thank Jennifer Lock for her efforts in developing and refining the Future ATM Concepts Evaluation Tool (FACET) Application Programming Interface, which was significantly leveraged in completing this study.

References

[1] Idris, H., Evans, A., Vivona, R., Krozel, J., and Bilimoria, K., "Field Observations of Interactions Between Traffic Flow Management and Airline Operations," AIAA 6th Aviation, Technology, Integration, and Operations Conference, Wichita, KS, AIAA Paper 2006-7721, Sept. 2006.

[2] Ball, M. O., Hoffman, R., Chen, C. Y., and Vossen, T., "Collaborative Decision Making in Air Traffic Management: Current and Future Research Directions," *New Concepts and Methods in Air Traffic Management*, edited by Bianco, L., Dell'Olmo, P., and Odoni, A. R., Springer–Verlag, New York, 2001.

[3] "*Enhanced Traffic Management System (ETMS)*," U.S. Dept. of Transportation, Volpe National Transportation Center, Rept. VNTSC-DTS56-TMS-002, Cambridge, MA, Oct. 2005.

[4] "Facility Operation and Administration," U.S. Dept. of Transportation, Federal Aviation Administration, Order JO 7210.3V, 14 Feb. 2008.

[5] "Concept of Operations for the Next Generation Air Transportation System, Version 2.0," Joint Planning and Development Office, http://www.jpdo.gov/library/NextGen_v2.0.pdf [retrieved 15 July 2008].

[6] Sridhar, B., Chatterji, G. B., Grabbe, S., and Sheth, K., "Integration of Traffic Flow Management Decisions," AIAA Guidance, Navigation, and Control Conference, Monterey, CA, AIAA Paper 2002-5014, Aug. 2002.

[7] Kopardekar, P., and Green, S., "Airspace Restriction Planner for Sector Congestion Management," AIAA Aviation, Technology, Integration, and Operations Conference, Arlington, VA, AIAA Paper 2005-7435, Sept. 2005.

[8] Bertsimas, D., and Patterson, S. S., "The Air Traffic Flow Management with En Route Capacities," *Operations Research*, Vol. 42, No. 3, 1994, pp. 249–261.

[9] Wanke, C., and Greenbaum, D., "Incremental Probabilistic Decision Making for En Route Traffic Management," *Air Traffic Control Quarterly*, Vol. 15, No. 4, 2007, pp. 299–319.

[10] Grabbe, S., Sridhar, B., and Mukherjee, A., "Sequential Traffic Flow Optimization with Tactical Flight Control Heuristics," AIAA Guidance, Navigation, and Control Conference, Honolulu, HI, AIAA Paper 2008-6823, Aug. 2008.

[11] Grabbe, S., Sridhar, B., and Mukherjee, A., "Central East Pacific Flight Scheduling," AIAA Guidance, Navigation, and Control Conference, Hilton Head, SC, AIAA, Paper 2007-6447, Aug. 2007.

[12] Cormen, T. H., Leiserson, C. E., Rivest, R. L., and Stein, C., *Introduction to Algorithms*, 2nd ed., MIT Press, Cambridge, MA, 2001.

[13] DeLaura, R., and Evans, J., "An Exploratory Study of Modeling En Route Pilot Convective Storm Flight Deviation Behavior," *12th American Meteorological Society Conference on Aviation, Range, and Aerospace Meteorology*, Atlanta, GA, American Meteorological Society, 2006, p. 12.6.

[14] Bilimoria, K. D., Sridhar, B., Chatterji, G. B., Sheth, K. S., and Grabbe, S. R., "FACET: Future ATM Concepts Evaluation Tool," *Air Traffic Control Quarterly*, Vol. 9, No. 1, 2001.

[15] Krozel, J., Penny, S., Prete, J., and Mitchell, J. S. B., "Comparison of Algorithms for Synthesizing Weather Avoidance Routes in Transition Airspace," AIAA Guidance, Navigation, and Control Conference, Providence, RI, AIAA, Paper 2004-4790, Aug. 2004.

[16] Krozel, J., Penny, S., Prete, J., and Mitchell, J. S. B., "Automated Route Generation for Avoiding Deterministic Weather in Transition Airspace," *Journal of Guidance, Control, and Dynamics*, Vol. 30, No. 1, 2007, pp. 144–153. doi:10.2514/1.22970

[17] Prete, J., and Mitchell, J. S. B., "Safe Routing of Multiple Aircraft Flows in the Presence of Time-Varying Weather Data," AIAA Guidance, Navigation, and Control Conference, Providence, RI, AIAA Paper 2004-4791, Aug. 2004.

[18] Ramamoorthy, K., Boisvert, B., and Huner, G., "A Real-Time Probabilistic Traffic Flow Management Evaluation Tool," *2006 IEEE/AIAA 25th Digital Avionics Systems Conference*, Inst. of Electrical and Electronics Engineers, Piscataway, NJ, Oct. 2006, pp. 1–13. doi:10.1109/DASC.2006.313783

[19] "Operational Data Reporting Requirements," U.S. Dept. of Transportation, Federal Aviation Administration, Order JO 7210.55E, 1 Oct. 2008.

[20] Krozel, J., Mitchell, J., Polishchuk, V., and Prete, J., "Capacity Estimation for Airspace with Convective Weather Constraints," AIAA Guidance, Navigation and Control Conference, Hilton Head, SC, AIAA Paper 2007-6451, Aug. 2007.

[21] Martin, B. D., "Model Estimates of Traffic Reduction in Storm Impacted En Route Airspace," AIAA Aviation, Technology, Integration, and Operations Conference, Arlington, VA, AIAA Paper 2007-7889, Sept. 2007.

[22] Rhoda, D., and Pawlak, M., "The Thunderstorm Penetration / Deviation Decision in the Terminal Area," *8th Conference on Aviation, Range, and Aerospace Meteorology*, American Meteorological Society, Jan., 1999, pp. 308–312.

[23] DeLaura, R., and Allan, S., "Route Selection Decision Support in Convective Weather: A Case Study of the Effects of Weather and Operational Assumptions on Departure Throughput," 5th Eurocontrol/ FAA ATM R&D Seminar, Eurocontrol Paper 73, 2003.

[24] Rhoda, D. A., Kocab, E. A., and Pawlak, M. L., "Aircraft Encounters with Convective Weather in En Route Vs. Terminal Airspace Above Memphis, Tennessee," *10th Conference on Aviation, Range and Aerospace Meteorology*, Portland, OR, American Meteorological Society, 2002, p. 5.13.

[25] Kuhn, K., "Analysis of Thunderstorm Effects on Aggregated Aircraft Trajectories," *Journal of Aerospace Computing, Information, and Communication*, Vol. 5, No. 4, pp. 108–119, 2008.

[26] Song, L., Wanke, C., Greenbaum, D., Zobell, S., and Jackson, C., "Methodologies for Estimating the Impact of Severe Weather on Airspace Capacity," 26th Congress of International Council of the Aeronautical Sciences (ICAS), Anchorage, AK, AIAA Paper 2008-8917, Sept. 2008.

[27] Mogford, R., Guttman, J., Morrow, S., and Kopardekar, P., "The Complexity Construct in Air Traffic Control: A Review and Synthesis of the Literature," FAA Technical Center, Rept. DOT/FAA/CT-TN-95/ 22, Atlantic City, NJ, 1995.